Ocean Systems Engineering, *Vol. 7, No. 1 (2017) 53–74*
DOI: https://doi.org/10.12989/ose.2017.7.1.053

A comparative assessment of approximate methods to simulate second order roll motion of FPSOs

Abhilash Somayajula* and Jeffrey Falzarano[a]

Department of Ocean Engineering, Texas A&M University, College Station, TX - 77840, USA

(Received December 26, 2015, Revised January 2, 2016, Accepted January 15, 2016)

Abstract. Ship shaped FPSO (Floating Production, Storage and Offloading) units are the most commonly used floating production units to extract hydrocarbons from reservoirs under the seabed. These structures are usually much larger than general cargo ships and have their natural frequency outside the wave frequency range. This results in the response to first order wave forces acting on the hull to be negligible. However, second order difference frequency forces start to significantly impact the motions of the structure. When the difference frequency between wave components matches the roll natural frequency, the structure experiences a significant roll motion which is also termed as second order roll.

This paper describes the theory and numerical implementation behind the calculation of second order forces and motions of any general floating structure subjected to waves. The numerical implementation is validated in zero speed case against the commercial code OrcaFlex. The paper also describes in detail the popular approximations used to simplify the computation of second order forces and provides a discussion on the limitations of each approximation.

Keywords: second order roll; FPSO roll; newman approximation; potential theory; OrcaFlex; KVLCC2; Quadratic Transfer Function (QTF)

1. Introduction

With the discovery of vast oil and natural gas reserves under the oceans, the number of deep water floating production units deployed to extract these hydrocarbons has increased by many folds in the last decade. Currently there are more than 250 floating production units around the world, of which more than 60 % are FPSOs. Although FPSOs have been built in different shapes and sizes, the ship shaped hull form is the most common owing to the cheaper conversion of old tankers into FPSOs.

FPSOs are usually huge structures designed such that their natural frequency is outside the wave frequency range (usually 2-20 seconds). This helps the structure to be relatively stable and allows for drilling and production operations to be performed on-board (Molin 2002).

In the recent years, a large number of FPSOs have been deployed near Western Africa and off the coast of Brazil. These environments are characterized by milder seas superimposed with long period

*Corresponding author, Ph.D., E-mail: s.abhilash89@gmail.com
[a]Ph.D., E-mail: jfalzarano@civil.tamu.edu

http://www.techno-press.org/?journal=sem&subpage=8 ISSN: 1225-4568(Print), 1598-6217(Online)

swells and are quite different than the North Atlantic or Gulf of Mexico environments. It has been observed that some of these deployed FPSOs exhibit a significant amount of roll motion in operating conditions (Ferreira *et al.* 2005). Higher roll amplitudes directly affect the fatigue life of the risers, ability to offload cargo, efficiency of process equipment and operations. For this reason, there is a renewed interest to understand the mechanism behind this phenomenon of second order roll motion (Rezende 2012).

The traditional approach to simulate this type of roll motion is to include the second order difference and sum frequency effects in addition to the linear diffraction and radiation forces. The second order forces and moments are described in terms of Quadratic Transfer Functions (QTF) which require solving both the first and second order potential problem using boundary element methods.

The second order forces and moments can be separated into two components (Chakrabarti 2002):

1. The contribution due to first order quantities computed at bi-chromatic frequencies which can further be classified into four parts
2. The contribution due to integration of second order diffraction potential over body surface up to mean water level

Since the first part is evaluated using first order quantities, it requires solving only the boundary value problem corresponding to the first order radiation and diffraction potentials. However, to evaluate the second order diffraction potential, a second boundary value problem needs to be solved. This problem has been investigated in detail by many researchers including Newman (1974), Pinkster (1980), Lee (1995) and Chen (2007). This approach has also been used by the industry to analyze practical problems (see for e.g., Liu 2003, Matsumoto and Simos 2014). However, in particular, when only the difference frequency drift forces are important, the problem can be approximated to reduce calculation time of QTF (Chen and Rezende 2009). While these approximations come at a cost of accuracy of the evaluated QTF, they have the advantage of being computationally cheap (Rezende and Chen 2010). Hauteclocque *et al.* (2012) provide a review of the different forms of approximation used to simplify the computation of difference frequency QTF.

This paper describes the implementation of the further development of in-house frequency (MDL-HydroD - Guha *et al.* 2016) and time domain (SIMDYN - Somayajula and Falzarano 2015a) simulation tools to include the slowly varying drift forces and moments. While the previous implementation of these tools could be used to analyze complex nonlinear phenomenon such as parametric roll (Somayajula and Falzarano 2016c, Somayajula *et al.* 2014, Somayajula and Falzarano 2015b) and also compute added resistance in both deep and shallow water (Guha *et al.* 2016), it still cannot include slowly varying drift forces and moments into the analysis.

This paper attempts to compare the various forms of Newman approximation to compute the difference frequency QTF. Also the second order force and moment are converted into time domain and compared against a commercial program for validation. Finally, the developed tool and commercial program are applied to simulate second order roll motion of a FPSO hull form and the roll time histories are compared for validation of the implementation. For the purpose of investigation of second order roll of FPSOs, the hull form of KVLCC2 (whose hull form and particulars are freely available) is selected as a candidate hull form and most of the results in this paper correspond to it. The particulars of KVLCC2 are listed in Table 1 and the body plan is shown in Fig. 1.

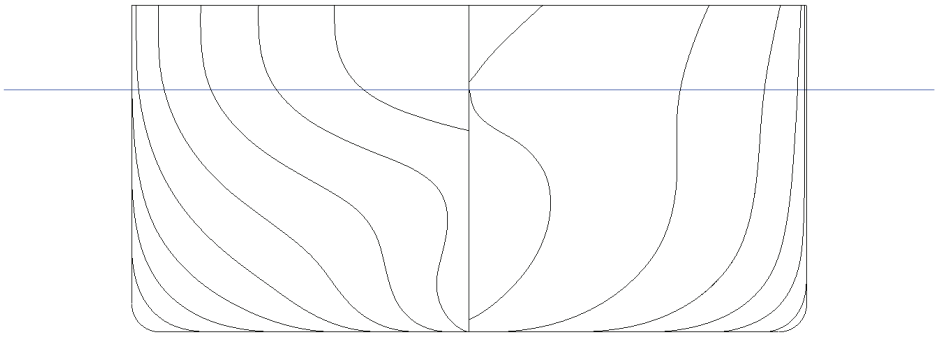

Fig. 1 Body Plan of KVLCC2

Table 1 Details of the KVLCC2

Particulars	**Value**
Length between perpendiculars L_{pp} (m)	320.00
Breadth B (m)	58.00
Depth D (m)	30.00
Mean Draft T (m)	20.80
Displacement Δ (tonnes)	320438
Vertical Center of Gravity $\overline{KG}$ (m)	18.205
Metacentric Height $\overline{GM}_t$ (m)	5.703
Roll Natural Period T_n (sec)	21.02

2. Potential theory

This section gives a brief overview of the potential theory formulation and application of perturbation method to approximate the problem. Finally, expressions for second order force and moment are obtained which form the main focus of the paper. Three sets of coordinate systems as assumed and are listed below.

1. **Global Earth Fixed Coordinate System (GCS)** which is fixed to the earth and is an inertial frame of reference. The coordinates of any point in this system are specified as $\boldsymbol{x_0} = (x_0, y_0, z_0)$.
2. **Steady Moving Coordinate System (SMCS)** is also an inertial frame of reference which moves with a constant velocity $\boldsymbol{U} = U\hat{i} + 0\hat{j} + 0\hat{k}$ with respect to GCS. The coordinates of any point in SMCS are specified as $\boldsymbol{x} = (x, y, z)$.

3. **Body Fixed Coordinate System (BCS)** is fixed with the body. This coordinate system translates and rotates with the ship. The coordinates of any point in BCS are specified as $\boldsymbol{x'} = (x', y', z')$.

Throughout this analysis it is assumed that the sinkage and trim in steady forward speed are negligibly small and are ignored. This means that the BCS and SMCS coincide for a ship moving steadily in calm water with velocity $\boldsymbol{U}$. A wave of unit amplitude, frequency ω_I and wave number k_I is assumed to be propagating at an angle β measured anticlockwise from the positive x-axis of GCS. Due to the steady forward speed of the ship, the frequency of wave encountered in SMCS undergoes a Doppler shift. This encounter frequency ω_e is higher than the incident wave frequency ω_I for $U > 0$ and $\frac{\pi}{2} < \beta < \frac{3\pi}{2}$. The encounter frequency ω_e is related to the incident wave frequency ω_I as shown in Eq. (1)

$$\omega_e = \omega_I - k_I U \cos\beta \tag{1}$$

For an inviscid and irrotational flow, there exists a complex velocity potential $\Phi(\boldsymbol{x}, t)$ in the entire fluid domain. $\Phi(\boldsymbol{x}, t)$ is defined in SMCS and is given by

$$\begin{aligned}\Phi(\boldsymbol{x}, t) = &- Ux + \underbrace{\phi_{St}(\boldsymbol{x})}_{\text{Neglect}} + \phi_I(\boldsymbol{x}, \omega_I, \beta) \\ &+ \phi_S(\boldsymbol{x}, \omega_I, \beta) + \sum_{i=1}^{6} \xi_i \phi_i(\boldsymbol{x}, \omega_e, \beta)\end{aligned} \tag{2}$$

where

- $\phi_{St}(\boldsymbol{x})$ is the potential due to the perturbation of the free stream due to the presence of the body and is called the steady potential
- $\phi_I(\boldsymbol{x}, \omega_I, \beta)$ is the wave potential due to the incident wave of frequency ω_I at an angle β and is called the incident wave potential
- $\phi_S(\boldsymbol{x}, \omega_I, \beta)$ is the wave potential due to the reflection of the incident waves from the body and is called the scattering wave potential
- $\phi_i(\boldsymbol{x}, \omega_e, \beta)$ is the potential due the waves generated by the unit amplitude motion of the ship in the i^{th} mode ($|\xi_i| = 1$)

Neglecting the effect of steady potential, $\Phi(\boldsymbol{x}, t)$ is given by

$$\Phi(\boldsymbol{x}, t) = - Ux + \phi \tag{3}$$

where

$$\phi = \phi_I(\boldsymbol{x}, \omega_I, \beta) + \phi_S(\boldsymbol{x}, \omega_I, \beta) + \sum_{i=1}^{6} \xi_i \phi_i(\boldsymbol{x}, \omega_e, \beta) \tag{4}$$

Governing Equation: Under the assumption of inviscid and irrotational flow, the governing Navier-Stokes equation reduces to the Laplace equation shown in Eq. (5) and is valid over the entire fluid domain

$$\nabla^2 \Phi(\boldsymbol{x}, t) = 0 \tag{5}$$

Boundary Conditions: In addition to satisfying the governing Laplace equation, the velocity potential must also satisfy the boundary conditions over the fluid boundaries. These include the following:

1. Kinematic free surface boundary condition: Velocity of the fluid in the direction normal to free surface is equal to the normal velocity of the free surface.

$$\frac{\partial \eta}{\partial t} = \frac{\partial \phi}{\partial z} - \left(-U + \frac{\partial \phi}{\partial x}\right)\frac{\partial \eta}{\partial x} - \frac{\partial \phi}{\partial y}\frac{\partial \eta}{\partial y} \quad \text{over } z = \eta(t, x, y) \tag{6}$$

2. Dynamic free surface boundary condition: Pressure on the free surface is constant $C = 0$ and is obtained by application of Bernaulli's equation over the free surface.

$$\begin{aligned} \frac{\partial \phi}{\partial t} + \frac{1}{2}\left\{ \left(-U + \frac{\partial \phi}{\partial x}\right)^2 + \left(\frac{\partial \phi}{\partial y}\right)^2 + \left(\frac{\partial \phi}{\partial z}\right)^2 \right\} \\ + g\eta = 0 \text{ over } z = \eta(t, x, y) \end{aligned} \tag{7}$$

3. Body boundary condition: Velocity of the fluid in the direction normal to body boundary is equal to the normal velocity of the body boundary over instantaneous underwater surface S.

$$(\boldsymbol{V}_s - \nabla \boldsymbol{\Phi}).\hat{\boldsymbol{n}} = 0 \tag{8}$$

The velocity of ship surface $\boldsymbol{V}_s$ at a point $\boldsymbol{x}$ on the underwater ship surface S is equal to the sum of the velocities induced due to translational and rotational motions of the ship.

$$\boldsymbol{V}_s = \dot{\boldsymbol{\xi}} + \boldsymbol{\omega} \times [\boldsymbol{x} - \boldsymbol{\xi}] \tag{9}$$

Thus the body boundary condition over the instantaneous wetted surface S is given by

$$\frac{\partial \phi}{\partial n} \equiv \nabla \phi.\hat{\boldsymbol{n}} = \left\{ \dot{\boldsymbol{\xi}} + \boldsymbol{\omega} \times (\boldsymbol{x} - \boldsymbol{\xi}) \right\}.\hat{\boldsymbol{n}} - \boldsymbol{W}.\hat{\boldsymbol{n}} \tag{10}$$

where $\boldsymbol{W} = \nabla(-Ux + \phi_{St})$ is the velocity vector due to the steady flow around the hull moving forward with speed U.

4. Bottom boundary condition: The normal velocity of the fluid at the bottom boundary is equal to the normal velocity of the boundary. For a impenetrable seabed in deep water the normal velocity is zero and the boundary condition is given by

$$\frac{\partial \phi}{\partial z} = 0 \text{ over the bottom } z = -\infty \tag{11}$$

5. Radiation boundary condition: This condition allows the locally generated waves to propagate outwards to ∞ in a fluid domain which is unbounded horizontally. This is also sometimes referred to as the Sommerfield radiation condition.

$$\lim_{r\to\infty} \sqrt{r}\left[\frac{\partial \phi_S}{\partial r} - ik\phi_S\right] = 0 \tag{12}$$

$$\lim_{r\to\infty} \sqrt{r}\left[\frac{\partial \phi_i}{\partial r} - ik\phi_i\right] = 0 \text{ for } i = 1, 2, ..., 6 \tag{13}$$

The free surface and body boundary condition are in general nonlinear and hence an exact analytical solution is not available. However, it is possible to adopt a perturbation approach to separate the problem into various orders of nonlinearity. The solution ϕ and other parameters of interest (wave elevation, pressure, normal vector, position vector) are expressed as a series expansion in terms of a small quantity ϵ (usually of the order of wave slope).

$$\phi = \epsilon\phi^{(1)} + \epsilon^2\phi^{(2)} + \epsilon^3\phi^{(3)} + ... \tag{14}$$
$$\eta = \epsilon\eta^{(1)} + \epsilon^2\eta^{(2)} + \epsilon^3\eta^{(3)} + ... \tag{15}$$
$$p = p^{(0)} + \epsilon p^{(1)} + \epsilon^2 p^{(2)} + \epsilon^3 p^{(3)} + ... \tag{16}$$
$$\hat{\boldsymbol{n}} = \hat{\boldsymbol{n}}^{(0)} + \epsilon\hat{\boldsymbol{n}}^{(1)} + \epsilon^2\hat{\boldsymbol{n}}^{(2)} + \epsilon^3\hat{\boldsymbol{n}}^{(3)} + ... \tag{17}$$
$$\boldsymbol{x} = \boldsymbol{x}^{(0)} + \epsilon\boldsymbol{x}^{(1)} + \epsilon^2\boldsymbol{x}^{(2)} + \epsilon^3\boldsymbol{x}^{(3)} + ... \tag{18}$$

The problem is thus reduced to solving a successive set of Laplace equations each with linearized boundary conditions. $\phi^{(1)}$ is obtained by solving the linearized problem shown below. The obtained solution of $\phi^{(1)}$ is further used in formulating the linearized problem for $\phi^{(2)}$ and so on.

$$\nabla^2\phi^{(1)} = 0 \tag{19}$$
$$\frac{\partial \eta^{(1)}}{\partial t} - U\frac{\partial \eta^{(1)}}{\partial x} = \frac{\partial \phi^{(1)}}{\partial z} \qquad \text{over } z = 0 \tag{20}$$
$$\frac{\partial \phi^{(1)}}{\partial t} - U\frac{\partial \phi^{(1)}}{\partial x} = -g\eta^{(1)} \qquad \text{over } z = 0 \tag{21}$$
$$\frac{\partial \phi^{(1)}}{\partial n} = \sum_{k=1}^{6} \dot{\xi}_k n_k + \xi_k m_k \qquad \text{over } S_0 \tag{22}$$

$$\frac{\partial \phi^{(1)}}{\partial z} = 0 \qquad \text{over } z = -\infty \tag{23}$$

where S_0 is the mean underwater hull surface and

$$(n_1, n_2, n_3) = \hat{\boldsymbol{n}}' \tag{24}$$
$$(n_4, n_5, n_6) = \boldsymbol{x}' \times \hat{\boldsymbol{n}}' \tag{25}$$
$$(m_1, m_2, m_3) = -(\hat{\boldsymbol{n}}'.\nabla)\boldsymbol{W} \tag{26}$$
$$(m_4, m_5, m_6) = -(\hat{\boldsymbol{n}}'.\nabla)(\boldsymbol{x}' \times \boldsymbol{W}) \tag{27}$$

and $\boldsymbol{W} \approx -U\hat{i} + 0\hat{j} + 0\hat{k}$ is the velocity vector due to the steady flow around the hull neglecting the effect of steady potential.

3. Second order forces and moments

The pressure at any point in the fluid is given by the Bernaulli's equation

$$\begin{aligned} p &= -\rho g z - \rho \frac{\partial \Phi}{\partial t} - \frac{\rho}{2} |\nabla \Phi|^2 \\ &= -\rho g z - \rho \frac{\partial \phi}{\partial t} + \rho U \frac{\partial \phi}{\partial x} - \frac{\rho U^2}{2} \\ &\quad - \frac{\rho}{2} \left\{ \left(\frac{\partial \phi}{\partial x} \right)^2 + \left(\frac{\partial \phi}{\partial y} \right)^2 + \left(\frac{\partial \phi}{\partial z} \right)^2 \right\} \end{aligned} \tag{28}$$

Redefining the pressure to be the gauge pressure the constant term $-\frac{\rho U^2}{2}$ can be removed from the dynamic pressure expression resulting in

$$p = -\rho g z - \rho \frac{\partial \phi}{\partial t} + \rho U \frac{\partial \phi}{\partial x} \quad - \frac{\rho}{2} \left\{ \left(\frac{\partial \phi}{\partial x} \right)^2 + \left(\frac{\partial \phi}{\partial y} \right)^2 + \left(\frac{\partial \phi}{\partial z} \right)^2 \right\} \tag{29}$$

Substituting $\phi = \epsilon\phi^{(1)} + \epsilon^2\phi^{(2)} + \epsilon^3\phi^{(3)} + ...$ and $z = z^{(0)} + \epsilon z^{(1)} + \epsilon^2 z^{(2)} + \epsilon^3 z^{(3)} + ...$ into the expression for pressure, exact expressions for various orders of pressure in terms of the potential can be obtained. The hydrodynamic force acting on the body is obtained by integrating the pressure over the wetted surface of the vessel

$$\boldsymbol{F} = \int_S p.\hat{\boldsymbol{n}} dS \tag{30}$$

$$\boldsymbol{M} = \int_S p.(\boldsymbol{x} \times \hat{\boldsymbol{n}}) dS \tag{31}$$

Applying a perturbation approach and substituting the perturbed expansion for pressure and normals, the hydrodynamic force and moment can be expressed as

$$\boldsymbol{F} = \boldsymbol{F}^{(0)} + \epsilon \boldsymbol{F}^{(1)} + \epsilon^2 \boldsymbol{F}^{(2)} + ... \tag{32}$$

$$\begin{aligned}\boldsymbol{F} = &\left(\int_{S_0} dS + \int_{wl} \zeta_r dl + ...\right)\left\{p^{(0)} + \epsilon p^{(1)} + \epsilon^2 p^{(2)} + ...\right\}. \\ &\left\{\hat{\boldsymbol{n}}' + \epsilon(\boldsymbol{\theta}^{(1)} \times \hat{\boldsymbol{n}}') + \epsilon^2 H\hat{\boldsymbol{n}}' + ...\right\}\end{aligned} \tag{33}$$

$$\boldsymbol{M} = \boldsymbol{M}^{(0)} + \epsilon\boldsymbol{M}^{(1)} + \epsilon^2\boldsymbol{M}^{(2)} + ... \tag{34}$$

$$\begin{aligned}\boldsymbol{M} = &\left(\int_{S_0} dS + \int_{wl} \zeta_r dl + ...\right)\left\{p^{(0)} + \epsilon p^{(1)} + \epsilon^2 p^{(2)} + ...\right\}. \\ &\left\{\boldsymbol{x}' \times \hat{\boldsymbol{n}}' + \epsilon\left[\boldsymbol{\xi}^{(1)} \times \hat{\boldsymbol{n}}' + \boldsymbol{\theta}^{(1)} \times (\boldsymbol{x}' \times \hat{\boldsymbol{n}}')\right]\right. \\ &\left. + \epsilon^2\left[H(\boldsymbol{x}' \times \hat{\boldsymbol{n}}') + \boldsymbol{\xi}^{(1)} \times (\boldsymbol{\theta}^{(1)} \times \hat{\boldsymbol{n}}')\right] + ...\right\}\end{aligned} \tag{35}$$

where the waterline integral $\int_{wl} \zeta_r dl$ appears due to the Taylor expansion of the integral on the instantaneous wetted surface S about the mean wetted surface S_0. ζ_r is the relative waterline and is given by

$$\zeta_r = \eta - (\xi_3 - \xi_5 x + \xi_4 y) \tag{36}$$

Note that $\boldsymbol{\xi}^{(1)} = \xi_1\hat{i} + \xi_2\hat{j} + \xi_3\hat{k}$ and $\boldsymbol{\theta}^{(1)} = \xi_4\hat{i} + \xi_5\hat{j} + \xi_6\hat{k}$ represent the first order displacement and rotation vectors and the matrix H represents the second order rotation matrix as defined in Eq. (37).

$$H = \begin{bmatrix} -\frac{1}{2}\left(\xi_5^2 + \xi_6^2\right) & 0 & 0 \\ \xi_4\xi_5 & -\frac{1}{2}\left(\xi_4^2 + \xi_6^2\right) & 0 \\ \xi_4\xi_6 & \xi_5\xi_6 & -\frac{1}{2}\left(\xi_4^2 + \xi_5^2\right) \end{bmatrix} \tag{37}$$

Expanding the terms and collecting the terms proportional to ϵ^2 in Eq. (33) and Eq. (35) results in expressions for the second order force and moment as shown in Eq. (38) and Eq. (39) respectively.

$$\begin{aligned}\boldsymbol{F}^{(2)} = &\int_{S_0} p^{(0)}\left(H\hat{\boldsymbol{n}}'\right) dS + \int_{S_0} p^{(1)}(\boldsymbol{\theta}^{(1)} \times \hat{\boldsymbol{n}}')dS \\ &+ \int_{S_0} p^{(2)}\hat{\boldsymbol{n}}' dS + \underbrace{\int_{wl} \zeta_r^{(1)} p^{(0)}(\boldsymbol{\theta}^{(1)} \times \hat{\boldsymbol{n}}')dl}_{=0 \text{ as } p^{(0)}=0 \text{ on } wl} + \int_{wl} \zeta_r^{(1)} p^{(1)}\hat{\boldsymbol{n}}' dl + \underbrace{\int_{wl} \zeta_r^{(2)} p^{(0)}\hat{\boldsymbol{n}}' dl}_{=0 \text{ as } p^{(0)}=0 \text{ on } wl}\end{aligned} \tag{38}$$

$$\begin{aligned}\boldsymbol{M}^{(2)} = & \int_{S_0} p^{(0)} \left[H(\boldsymbol{x}' \times \hat{\boldsymbol{n}}') + \boldsymbol{\xi}^{(1)} \times (\boldsymbol{\theta}^{(1)} \times \hat{\boldsymbol{n}}') \right] dS \\ & + \int_{S_0} p^{(1)} \left[\boldsymbol{\xi}^{(1)} \times \hat{\boldsymbol{n}}' + \boldsymbol{\theta}^{(1)} \times (\boldsymbol{x}' \times \hat{\boldsymbol{n}}') \right] dS + \int_{S_0} p^{(2)} \left(\boldsymbol{x}' \times \hat{\boldsymbol{n}}' \right) dS \\ & + \underbrace{\int_{wl} \zeta_r^{(1)} p^{(0)} \left[\boldsymbol{\xi}^{(1)} \times \hat{\boldsymbol{n}}' + \boldsymbol{\theta}^{(1)} \times (\boldsymbol{x}' \times \hat{\boldsymbol{n}}') \right] dl}_{=0 \text{ as } p^{(0)}=0 \text{ on } wl} \\ & + \int_{wl} \zeta_r^{(1)} p^{(1)} \left(\boldsymbol{x}' \times \hat{\boldsymbol{n}}' \right) dl + \underbrace{\int_{wl} \zeta_r^{(2)} p^{(0)} \left(\boldsymbol{x}' \times \hat{\boldsymbol{n}}' \right) dl}_{=0 \text{ as } p^{(0)}=0 \text{ on } wl}\end{aligned} \tag{39}$$

The second order force and moment obtained from perturbation theory accommodate interaction between two wave trains with different amplitudes and frequencies. The interaction between two regular waves (bi-chromatic waves) gives rise to forces and moments at difference and sum frequencies. The total second order force and moment denoted by Eq. (38) and Eq. (39) respectively are the sum of the forces and moments due to sum and difference frequency effects as represented below

$$\boldsymbol{F}^{(2)}(\omega_m, \omega_n) = \boldsymbol{F}^{(2d)}(\omega_m, \omega_n) + \boldsymbol{F}^{(2s)}(\omega_m, \omega_n) \tag{40}$$

$$\boldsymbol{M}^{(2)}(\omega_m, \omega_n) = \boldsymbol{M}^{(2d)}(\omega_m, \omega_n) + \boldsymbol{M}^{(2s)}(\omega_m, \omega_n) \tag{41}$$

where

- $\boldsymbol{F}^{(2s)}(\omega_m, \omega_n)$ is the sum frequency component of the second order force
- $\boldsymbol{F}^{(2d)}(\omega_m, \omega_n)$ is the difference frequency component of the second order force
- $\boldsymbol{M}^{(2s)}(\omega_m, \omega_n)$ is the sum frequency component of the second order moment
- $\boldsymbol{M}^{(2d)}(\omega_m, \omega_n)$ is the difference frequency component of the second order moment

If the two regular wave trains in a bi-chromatic wave have amplitudes A_m and A_n, a set of second order transfer functions can be defined as shown below. These transfer functions are also referred to as quadratic transfer functions (QTFs).

$$Q_i^{(2d)}(\omega_m, \omega_n) = \frac{F_i^{(2d)}(\omega_m, \omega_n)}{A_m A_n} \qquad \text{for } i = 1, 2, 3 \tag{42}$$

$$Q_i^{(2s)}(\omega_m, \omega_n) = \frac{F_i^{(2s)}(\omega_m, \omega_n)}{A_m A_n} \qquad \text{for } i = 1, 2, 3 \tag{43}$$

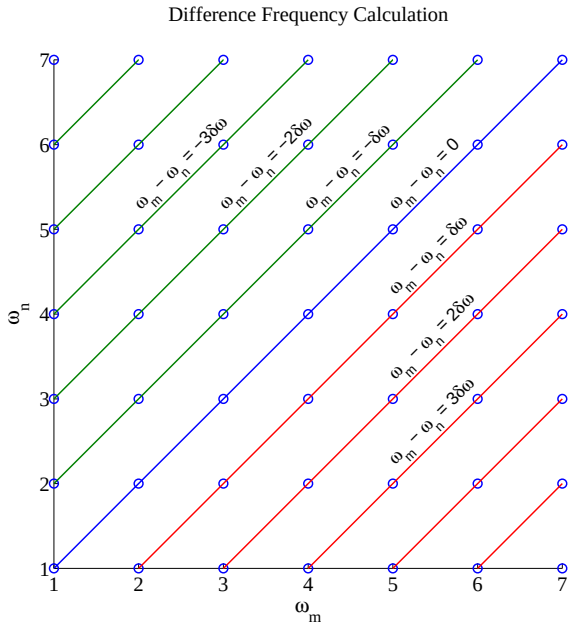

Fig. 2 Difference frequency pairs in bi-frequency (ω_m, ω_n) plane

$$Q_i^{(2d)}(\omega_m, \omega_n) = \frac{M_{i-3}^{(2d)}(\omega_m, \omega_n)}{A_m A_n} \qquad \text{for } i = 4, 5, 6 \tag{44}$$

$$Q_i^{(2s)}(\omega_m, \omega_n) = \frac{M_{i-3}^{(2s)}(\omega_m, \omega_n)}{A_m A_n} \qquad \text{for } i = 4, 5, 6 \tag{45}$$

4. Quadratic Transfer Function (QTF) approximations

Practically, the second order forces play an important role only when the natural frequency of the structure is outside the wave frequency zone where the first order forces are insignificant. If the natural frequency of a structure is higher than the wave frequency range, like a tension leg platform (TLP), then the sum frequency effects play a dominant role. However, for soft moored systems such as semi-submersibles and FPSOs, the difference frequency effects are most dominant. In analyzing the motions of a FPSO, the difference frequency effects are more important as the natural period is in the low frequency zone.

It can be seen from Eq. (38) and Eq. (39) that to evaluate the second order force and moment up to $O(\epsilon^2)$ requires computation of $p^{(2)}$ which in turn requires calculation of $\phi^{(2)}$. Thus for exact calculation, a second boundary value problem for $\phi^{(2)}$ needs to be solved. This makes obtaining exact values for $Q^{(2d)}(\omega_m, \omega_n)$ and $Q^{(2s)}(\omega_m, \omega_n)$ computationally expensive. In order to make the problem tenable Pinkster (1980) suggested replacing the total potential $\phi^{(2)}$ by the incident potential $\phi_I^{(2)}$ which is analytically known. The QTF calculated using this approach is know as the Pinkster's approximated QTF. Note that this still requires calculating the QTF for each of the frequency pairs in the bi-frequency plane.

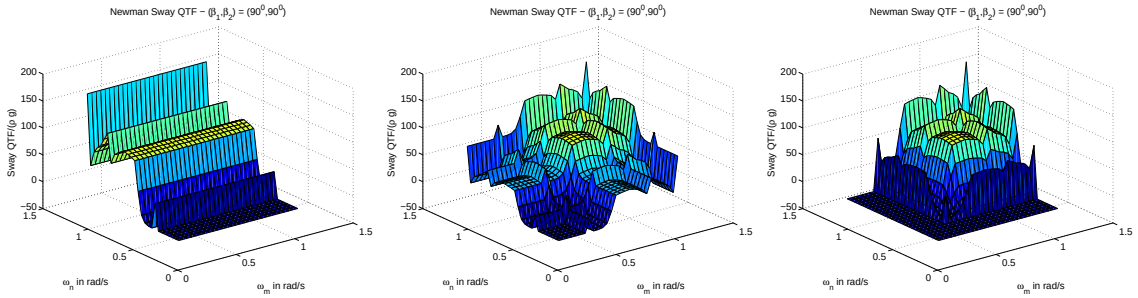

(a) Original (b) Arithmetic Mean (c) Geometric Mean

Fig. 3 Sway QTF using different Newman approximations

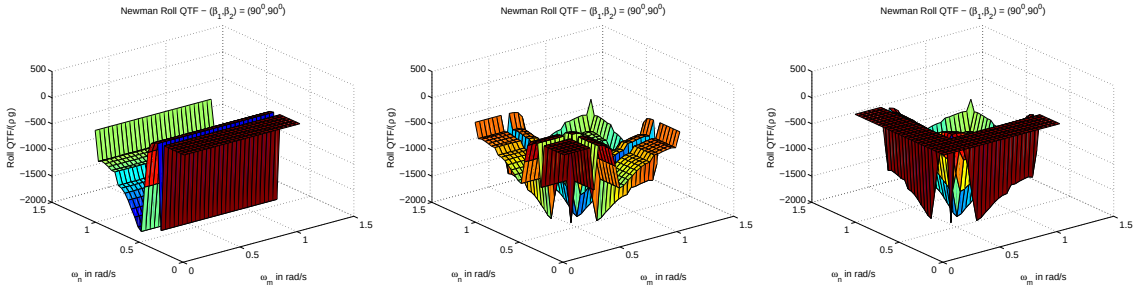

(a) Original (b) Arithmetic Mean (c) Geometric Mean

Fig. 4 Roll QTF using different Newman approximations

Practically, it is seen that the difference frequency QTFs have their largest contribution coming from frequency pairs on or near the diagonal $\omega_m - \omega_n = 0$ in the bi-frequency plane. The difference frequency diagonals are shown in Fig. 2. For such cases, Newman (1974) suggested an approximation of the QTF using a method which just requires the QTF values for the diagonal pairs. The diagonal represents the pair of frequencies where the difference frequency forces except for the terms involving the second order potential are constant terms. These constant values over the diagonal are termed as the mean drift forces. Newman approximation utilizes the mean drift forces to predict the QTF values for the off-diagonal frequency pairs. The original Newman approximation is given by Eq. (46)

$$Q^{(2d)}(\omega_m, \omega_n) = Q^{(2d)}(\omega_m, \omega_m) \tag{46}$$

However, other forms of Newman approximation which have become quite accepted include the arithmetic mean and geometric mean models shown in Eq. (47) and Eq. (48) respectively

$$Q^{(2d)}(\omega_m, \omega_n) = \frac{1}{2}\left(Q^{(2d)}(\omega_m, \omega_m) + Q^{(2d)}(\omega_n, \omega_n)\right) \tag{47}$$

$$Q^{(2d)}(\omega_m, \omega_n) = \text{sign}(Q^{(2d)})\sqrt{Q^{(2d)}(\omega_m, \omega_m)Q^{(2d)}(\omega_n, \omega_n)} \tag{48}$$

Fig. 3 and Fig. 4 shows a comparison of the sway and roll QTFs of KVLCC2 for incident bi-chromatic beam waves between the three forms of Newman approximations. The frequency domain program used in this investigation (MDLHYDROD developed by Guha and Falzarano 2015) only provides the output of mean drift coefficients and does not calculate QTF at each of the frequency pairs in bi-frequency plane. Thus the investigation in this section will be limited to using the different Newman approximation models to estimate the QTF. The output mean drift coefficients from the frequency domain program are used in SIMDYN to calculate the Newman approximated QTFs which are then used to generate the second order force and moment time series. The conversion from QTF to time series is described in the next section.

5. Numerical computation of second order forces and moments in time domain

For evaluating the motions of a vessel including the second order effects, the frequency domain formulation described in the previous section needs to be transformed into the time domain. A uni-directional irregular wave train in the time domain is represented by the inverse Fourier transform of the complex wave amplitudes generated from a spectrum as shown below

$$\eta(t) = \mathrm{Re}\left\{ \sum_{m=1}^{N} A_m e^{i\omega_m t} \right\} \tag{49}$$

where A_m is the complex wave amplitude (characterizing the amplitude and phase) of each of the N wave components in the wave train. It is also assumed that the frequencies ω_m are equally spaced between 0 and ω_N. The magnitude of amplitude is obtained from the spectrum by $|A_m| = \sqrt{2S(\omega_m)d\omega}$ and the phase is obtained from a uniform random variable which assumes values between 0 and 2π. Using this description of the waves in time domain, the second order forces and moments can be evaluated by

$$F_i^{(2)} = F_i^{(2d)} + F_i^{(2s)} \tag{50}$$

where $(*)$ represents complex conjugate and $F_i^{(2d)}(t)$ and $F_i^{(2s)}(t)$ are given by

$$\begin{aligned} F_i^{(2d)}(t) &= \mathrm{Re}\left\{ \sum_{m=1}^{N}\sum_{n=1}^{N} A_m A_n^* Q_i^{(2d)}(\omega_m, \omega_n) e^{i(\omega_m - \omega_n)t} \right\} \\ F_i^{(2s)}(t) &= \mathrm{Re}\left\{ \sum_{m=1}^{N}\sum_{n=1}^{N} A_m A_n Q_i^{(2s)}(\omega_m, \omega_n) e^{i(\omega_m + \omega_n)t} \right\} \end{aligned} \tag{51}$$

However, implementing this formulation necessitates taking a double inverse Fourier transform which is computationally expensive. However, utilizing the symmetry and observing that the pairs of (ω_m, ω_n) along the diagonals in bi-frequency plane correspond to same second order frequency components, an alternative scheme using a single inverse Fourier transform can be formulated. Since the focus of this paper is on difference frequency effects on roll motion, the formulation will be developed for the difference frequency QTF. A similar scheme can also be applied to evaluating the sum frequency forces and moments, but will not be discussed here. More details on numerically

implementing the alternative scheme for sum frequency forces and moments can be found in Duarte *et al.* (2014).

Fig. 2 shows the various frequency pairs which contribute to the same second order difference frequency component of the second order force/moment. Along each diagonal in Fig. 2 the difference between the frequency pairs is constant. The main diagonal $\omega_m - \omega_n = 0$ corresponds to zero difference frequency term or the mean term of the second order force/moment. The k^{th} off-diagonal to the right of the main diagonal in the bi-frequency plane corresponds to a difference frequency of $k\delta\omega$. The double summation in Eq. (51) can now be represented as sums across the diagonals in the bi-frequency plane. The double inverse Fourier transform (over ω_m and ω_n) in Eq. (51) is now reduced to a single inverse Fourier transform (over ω_k) as shown in Eq. (52)

$$F_i^{(2d)}(t) = \mathrm{Re}\Bigg\{ \underbrace{\sum_{p=1}^{N} A_p A_p^* Q^{(2d)}(\omega_p, \omega_p)}_{\text{Main Diagonal}} + \underbrace{2 \sum_{k=1}^{N-1} \overbrace{\left(\sum_{l=1}^{N-k} A_{l+k} A_l^* Q_i^{(2d)}(\omega_{l+k}, \omega_l) \right)}^{\text{Sum along each Off-Diagonal}} e^{i\omega_k t}}_{\text{Sum over Off-Diagonals}} \Bigg\} \tag{52}$$

The summations in the second term in Eq. (52) represent the contribution due to the off-diagonals to the right of the main diagonal in Fig. 2. The effect of the off-diagonals to the left of the main diagonal is equal to the contribution due to the off-diagonals towards the right of the main diagonal. This is due to the special property of the difference frequency QTF as shown below

$$Q^{(2d)}(\omega_n, \omega_m) = Q^{(2d)}(\omega_m, \omega_n)^* \tag{53}$$

Thus the contribution due to frequency pairs obtained by interchanging the frequencies is the same as shown below

$$\begin{aligned} &\mathrm{Re}\Big\{ A_m A_n^* Q^{(2d)}(\omega_m, \omega_n) e^{i(\omega_m - \omega_n)} \Big\} \\ &= \mathrm{Re}\Big\{ \left(A_m^* A_n Q^{(2d)}(\omega_m, \omega_n)^* e^{i(\omega_n - \omega_m)} \right)^* \Big\} \\ &= \mathrm{Re}\Big\{ \left(A_n A_m^* Q^{(2d)}(\omega_n, \omega_m) e^{i(\omega_n - \omega_m)} \right)^* \Big\} \\ &= \mathrm{Re}\Big\{ A_n A_m^* Q^{(2d)}(\omega_n, \omega_m) e^{i(\omega_n - \omega_m)} \Big\} \end{aligned} \tag{54}$$

SIMDYN has been developed to include the option to choose which Newman approximation to use. This allows for a comparison of the second order moment in time domain using the different approximations. Fig. 5 shows the comparison of roll drift moment obtained using the three different Newman approximations described in the previous section. It can be seen that in a deep water scenario all three approximations are almost equivalent.

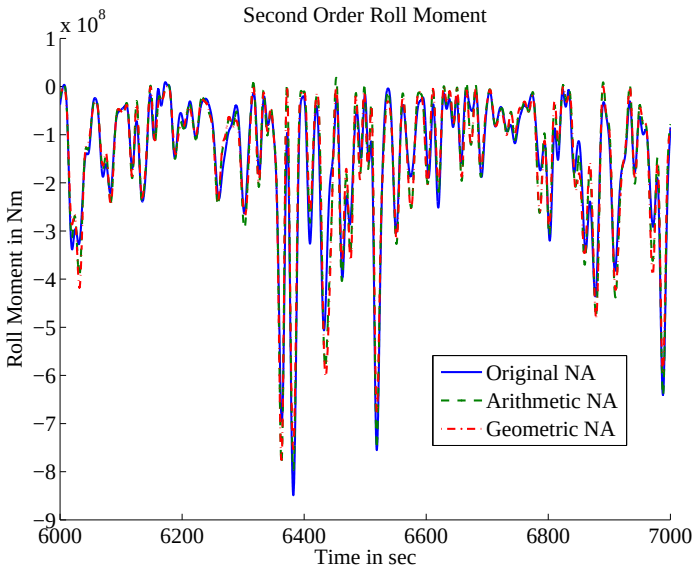

Fig. 5 Comparison of second order roll moment using different Newman approximations for KVLCC2 hull subjected to irregular beam sea realization from JONSWAP spectrum with significant wave height $H_s = 7$ m and modal period $T_z = 7$ s

6. Validation studies

The above described method to calculate the second order forces and moments is numerically implemented into the time domain program SIMDYN described in Somayajula and Falzarano (2015a). However care is taken to avoid any double counting of the hydrodynamic forces. The second order forces and moments and the nonlinear Froude-Krylov and hydrostatics (described in Somayajula and Falzarano 2015a) cannot be considered together as it would result in double counting. Thus when the second order forces and moments are included in analysis only linear Froude Krylov and hydrostatics are additionally included. Once the force and moment time series are obtained, the resulting motions are solved for using a numerical integration scheme described in Somayajula and Falzarano (2015a). For zero speed case, the results from SIMDYN are validated against a commercial software OrcaFlex. Although the combination of MDLHYDROD and SIMDYN can handle forward speed case, it cannot be compared with OrcaFlex as it cannot perform calculations for forward speed.

Note that although SIMDYN has a viscous roll damping calculation included, no viscous roll damping has been used in this study to achieve large roll angles for effective comparison between the two programs. In reality, the viscous damping coefficients are either obtained from free decay experiments or empirical methods (Himeno 1981, Falzarano *et al.* 2015). In the event of unavailability of free decay experiments, the damping can also be identified from model tests in irregular seas using system identification techniques (see for e.g., Somayajula and Falzarano 2016a, b)

Fig. 6a shows a comparison of the second order roll moment due to bichromatic incident beam waves with wave heights $H_1 = 7$ m, $H_2 = 8$ m and wave periods $T_1 = 7$ s, $T_2 = 10.75$ s. A similar comparison for the case of irregular wave from JONSWAP spectrum superimposed on a regular wave is shown in Fig. 6b

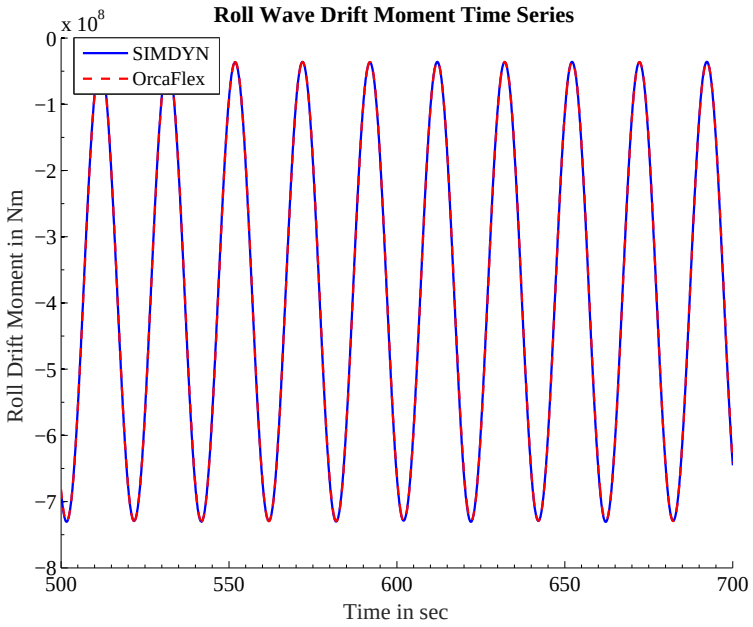

(a) Bi-chromatic incident beam waves with two regular wave components with wave heights $H_1 = 7$ m, $H_2 = 8$ m and wave periods $T_1 = 7$ s, $T_2 = 10.75$ s

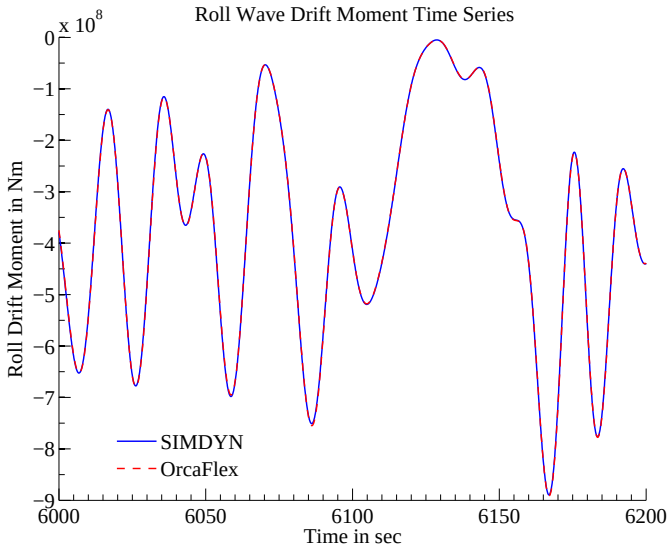

(b) Irregular beam sea realization from JONSWAP spectrum with significant wave height $H_s = 8$ m and modal period $T_z = 7$ s superimposed with a regular wave $H = 7$ m and $T = 11$ s

Fig. 6 Second order roll drift moment of KVLCC2

In each of the two examples shown in Figure 6, the example is first setup in OrcaFlex. After the OrcaFlex simulation is completed, the wave profile from OrcaFlex simulation is retrieved and used as an input to SIMDYN simulation. It can be seen that the results compare very well in both regular and irregular wave scenarios.

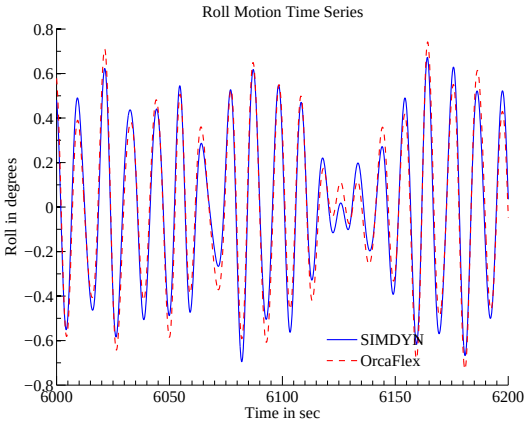

Fig. 7 Comparison of linear roll motion of KVLCC2 between OrcaFlex and SIMDYN

The comparison of linear roll motion between OrcaFlex and SIMDYN for KVLCC2 ship subject to a beam sea realization from JONSWAP spectrum with significant height $H_s = 8$ m and modal period $T_z = 7$ s superimposed on a regular wave of height $H = 7$ m and period $T = 11$ s is shown in Figure 7. Note that the nonlinear second order roll moment is not included in the calculation of roll motion. Since the roll natural frequency is outside the wave frequency zone, the roll response is significantly low.

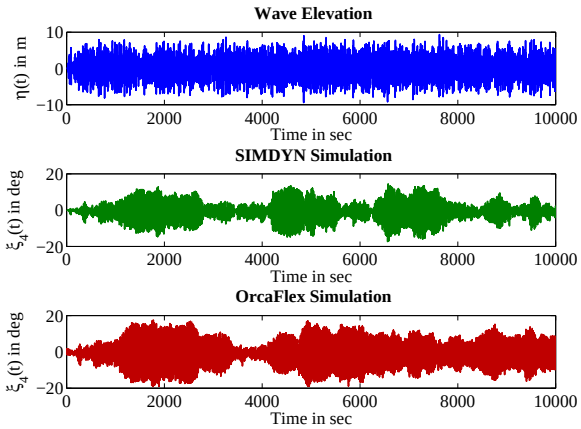

Fig. 8 Comparison of second order roll motion of KVLCC2 between OrcaFlex and SIMDYN

However including the nonlinear second order roll moment into the force vector results in significantly larger roll response and is shown in Fig. 8. A comparison within a smaller 1000 second window is also shown in Fig. 9. The comparison of roll motion between SIMDYN and OrcaFlex in

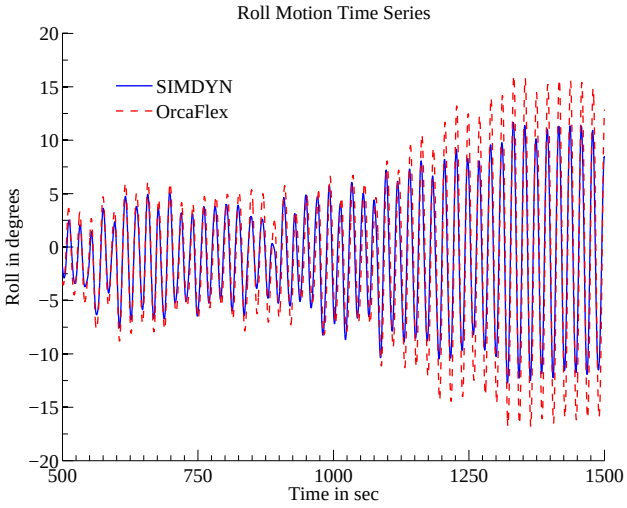

Fig. 9 Comparison of second order roll motion of KVLCC2 between OrcaFlex and SIMDYN

case irregular seas shows that the motion comparison is somewhat reasonable but not an exact match. Although the two time series agree well at the beginning, they quickly diverge from each other as seen in Fig. 9.

Since the external roll moment and all the particulars are the same between the two cases (see Fig. 6), the only possible difference is in the inclusion of radiation forces in time domain. While the frequency dependent added mass and radiation damping have a physical meaning in regular wave scenario, for the irregular wave case they need to be transformed into the impulse response functions (also known as retardation functions) for computation in the time domain. The radiation force vector in the time domain is given by Eq. (55)

$$\{F_{rad}\} = -[A(\infty)]\{\ddot{\xi}\} - \int_{-\infty}^{t} [K(t-\tau)]\{\dot{\xi}(\tau)\}d\tau \tag{55}$$

where $\{\xi\}$ represents the 6×1 displacement vector, $[A(\infty)]$ denotes the 6×6 infinite frequency added mass matrix and $[K(\tau)]$ represents the 6×6 impulse response functions (IRF). The IRFs are usually calculated from the radiation damping using Eq. (56)

$$[K(\tau)] = \frac{2}{\pi}\int_{0}^{\infty} [B(\omega) - B(\infty)]\cos(\omega\tau)d\omega \tag{56}$$

The accuracy of the calculated IRF depends on the computation of the improper integral shown in Eq. (56). The input frequency domain data for both programs is only provided at a set of discreet frequencies. Therefore it is common to assume a decaying functional tail for the radiation damping at higher frequencies and include it in the computation of the improper integral shown in Eq. (56). OrcaFlex uses a ω^{-3} tail approximation. However, SIMDYN uses a ω^{-2} tail based on the classical works of Greenhow (1986) and Perez and Fossen (2008). This means that SIMDYN uses a slower decaying tail and hence will result in higher damping as compared to OrcaFlex. This is illustrated in Fig. 10 which shows the comparison of the impulse response function for the roll mode computed

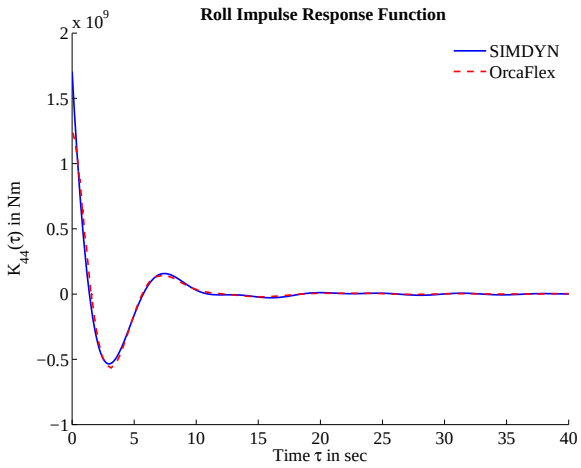

Fig. 10 Comparison of Roll IRF calculated from SIMDYN and OrcaFlex

from both programs. Although both IRFs converge in the tail region, SIMDYN IRF has a higher value at $\tau = 0$ which clearly indicates the higher damping introduced by the heavier tail function assumed.

Another point of difference between the two programs is the computation of infinite frequency added mass matrix. SIMDYN uses the exact infinite frequency added mass computed from the frequency domain formulation. However, OrcaFlex does not take an input for the infinite added mass matrix. It instead calculates the infinite frequency added mass matrix by using the added mass at a given frequency and the impulse response function matrix. The relation is shown in Eq. (57) and the theory behind it is described in detail in Somayajula and Falzarano (2015a). It calculates an estimate using data for each specified input frequency and finally takes an average of all the estimates to arrive at the final infinite frequency added mass which is then used in solving the equation of motion. However, in this particular example it was found that the infinite frequency added mass in roll $A_{44}(\infty)$ calculated by this method was only 0.33% different from that provided directly by the frequency domain program. Note that effect of this difference does not show up in the second order forces or moments but only comes up when the motions are solved for numerically

$$[A(\infty)] = [A(\omega)] + \frac{1}{\omega}\int_0^\infty [K(\tau)]\sin(\omega\tau)d\tau \tag{57}$$

With these differences in the computation of radiation force vector, one would assume that in case of no external damping, the motions predicted by SIMDYN would be less as compared to OrcaFlex as is seen in Figs. 8 and 9.

6.1 Second order forces in forward speed

The example considered in the above sections is a zero forward speed case. However, the current development of the program allows for the calculation of second order forces in forward speed too. Since OrcaFlex cannot handle non-zero forward speed of the vessel, the second order forces in non-zero forward speed case cannot be compared with it. As the forward speed formulation is still based

Table 2 Details of the S175 container ship

Particulars	**Value**
Length between perpendiculars L_{pp} (m)	175.00
Breadth B (m)	25.40
Mean Draft T (m)	9.50
Displacement Δ (tonnes)	25266
Vertical Center of Gravity $\overline{KG}$ (m)	9.50
Roll Natural Period T_n (sec)	18.70

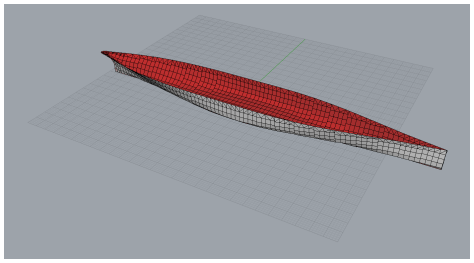

Fig. 11 Underwater mesh for S175 container ship

off a zero speed Green function, a finer hull form S175 container ship is chosen to satisfy the slender assumption. The particulars of S175 container ship are listed in Table 2. The underwater mesh of the vessel used to calculate the frequency domain data is shown in Fig. 11.

The comparison of the zero and forward speed added resistance in frequency domain (from MDL-HYDROD program) is shown in Fig. 12. The comparison of forward speed added resistance in frequency domain against experiments can be found in the works of Guha and Falzarano (2015). The added resistance QTF for head sea case is shown in Fig. 13 and the corresponding time history of second order surge added resistance experienced in an irregular wave realized from JONSWAP spectrum is shown in Fig. 14.

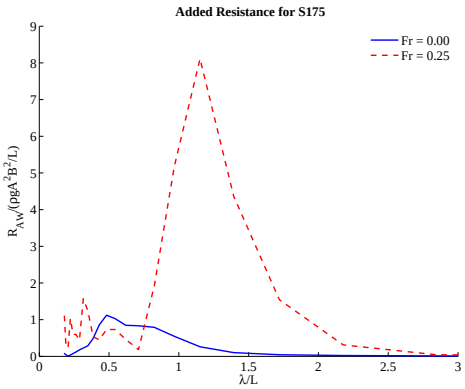

Fig. 12 Frequency domain added resistance for S175 container ship in head seas

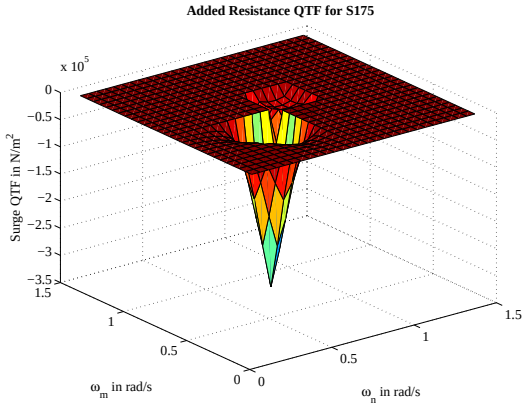

Fig. 13 Added Resistance QTF for head seas for S175 container ship ($Fr = 0.25$)

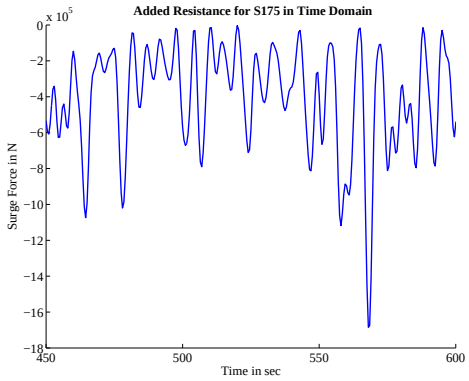

Fig. 14 Added Resistance for S175 container ship in a JONSWAP spectrum wave realization with significant wave height $H_s = 8$ m and peak period $T_p = 14$ s ($Fr = 0.25$)

7. Conclusions

In this paper the time domain simulation program developed in Somayajula and Falzarano (2015a) has been extended to include the second order difference frequency forces and moments in addition to the linear Froude Krylov and hydrostatics. Specifically, the work has focused around the use of the Newman approximation for predicting the QTF from just the mean drift coefficients. The different forms of the Newman approximation have been implemented and the corresponding results in both frequency domain and time domain have been compared. It has been found that all three forms of Newman approximation result in qualitatively similar results in the deep water case.

The developed formulation has been applied to the problem of second order roll motion of a FPSO excited by bi-chromatic and irregular beam seas. The developed approach has been validated by comparison with a commercial software OrcaFlex in the case of zero speed.

The current time domain simulation tool is capable of calculating the mean drift forces and moments in the case of forward speed. The force in the surge direction in case of forward speed is also known as added resistance. With the current formulation, added resistance of a structure can be

calculated in time domain. At present the current available commercial software, OrcaFlex, cannot predict the added resistance in time domain. One of the future investigations would be to compare the added resistance in time domain with either a commercial or another research code to validate the results.

Another proposed extension to the current stage would be to include the shallow water dispersion relation formulation and extend the capability of the time domain code to handle finite water depth scenario. This will provide an opportunity to compare the different forms of the Newman approximation for finite depth scenario where it is believed that the various approximations do not agree well with each other (Rezende *et al.* 2008).

Acknowledgements

The research described in this paper was funded by Chevron Energy Technology Company. This work was also partially supported by the Office of Naval Research (ONR)-ONR Grant N000-14-16-1-2281. The authors would like to thank Dr. Paul Hess for facilitating the funding from ONR. Special thanks needs to be mentioned to Dr. Amitava Guha for his assistance in comparison studies between SIMDYN with OrcaFlex.

References

Chakrabarti, S. (2002), *The theory and practice of hydrodynamics and vibration*, World Scientific, Singapore.

Chen, X.B. (2007), "Middle-field formulation for the computation of wave-drift loads", *J. Eng. Math.*, **59**(1), 61-82.

Chen, X.b. and Rezende, F. (2009), "Efficient computations of second-order low-frequency wave load", *Proceedings of the ASME 28th International Conference on Ocean, Offshore and Arctic Engineering* Volume 1: Offshore Technology, 525-532, ASME, URL http://proceedings.asmedigitalcollection.asme.org/proceeding.aspx?articleid=1622777.

Duarte, T., Sarmento, A.J.N.A. and Jonkman, J.M. (2014), *Effects of second-order hydrodynamic forces on floating offshore wind turbines*, Technical Report April, National Renewable Energy Laboratory.

Falzarano, J., Somayajula, A. and Seah, R. (2015), "An overview of the prediction methods for roll damping of ships", *Ocean Syst. Eng.*, **5**(2), 55-76.

Ferreira, M.D., Torres, F., Cueva, D., Ceppollina, D., Pinheiro, S., Jr, H.C. and Umeda, C. (2005), "Hydrodynamic aspects of the new build FPSOBR", *2nd International Conference on Applied Offshore Hydrodynamics*, Rio de Janerio.

Greenhow, M. (1986), "High-and low-frequency asymptotic consequences of the Kramers-Kronig relations", *J. Eng. Math.*, **20**, 293-306,

Guha, A. and Falzarano, J. (2015), "The effect of hull emergence angle on the near field formulation of added resistance", *Ocean Eng.*, **105**, 10-24.

Guha, A., Somayajula, A. and Falzarano, J. (2016), "Time domain simulation of large amplitude motions in shallow water", *21st SNAME Offshore Symposium*, February, Society of Naval Architects and Marine Engineers, Houston.

Hauteclocque, G.D., Rezende, F., Waals, O. and Chen, X.B. (2012), "Review of approximations to evaluate second-order low-frequency load", *Proceedings of the ASME 2012 31st International Conference on Ocean, Offshore and Arctic Engineering*, 1-9.

Himeno, Y. (1981), *Prediction of Ship Roll Damping-A State of the Art*, Technical Report 239, The University of Michigan, Ann Arbor.

Lee, C. (1995), *WAMIT theory manual*, Technical report, Massachusettes Institute of Technology, Cambridge, MA.

Liu, Y. (2003), "On Second-Order Roll Motions of Ships", *Proceedings of the ASME 2012 22nd International Conference on Offshore Mechanics and Arctic Engineering*, 1-6, American Society of Mechanical Engineers, Cancun, Mexico.

Matsumoto, F.T. and Simos, A.N. (2014), "Predicting the second order resonant roll motions of an FPSO", *Proceedings of the ASME 2014 33rd International Conference on Ocean, Offshore and Arctic Engineering*, 1-9, American Society of Mechanical Engineers, San Francisco, California, USA.

Molin, B. (2002), *Hydrodynamique des structures offshore*, Editions Technip, Paris.

Newman, J. (1974), "Second-order, slowly-varying forces on vessels in irregular waves", *International Symposium on Dynamics of Marine Vehicle & Structures in Waves*, 193-197, Mechanical Engineering Publications, London.

Perez, T. and Fossen, T. (2008), "A derivation of high-frequency asymptotic values of 3d added mass and damping based on properties of the cummins' equation", *J. Maritime Res.*, **5**(1), 65-78.

Pinkster, J.A. (1980), "Low frequency second order wave exciting forces on floating structures", Doctoral, Technische Universiteit Delft.

Rezende, F. (2012), *Non Linear Roll JIP*, Technical report, Bureau Veritas, Rio de Janerio.

Rezende, F., Chen, X.b.B. and Ferreira, M.D. (2008), "Simulation of second order roll motions of a FPSO", *Proceedings of the 27th International Conference on Offshore Mechanics and Arctic Engineering - 2008, Vol 1*, 355-361, American Society of Mechanical Engineers, Estoril, Portugal.

Rezende, F.C. and Chen, X.B. (2010), "Approximation of second-order low-frequency wave loading in multidirectional waves", *29th International Conference on Ocean, Offshore and Arctic Engineering: Volume 3*, 855-861, ASME.

Somayajula, A. and Falzarano, J. (2015a), "Large-amplitude time-domain simulation tool for marine and offshore motion prediction", *Marine Syst. Ocean Technol.*, **10**(1), 1-17.

Somayajula, A. and Falzarano, J. (2016a), "Critical assessment of reverse-MISO techniques for system identification of coupled roll motion of ships", *J. Marine Sci. Technol.*, 1-19.

Somayajula, A. and Falzarano, J. (2016b), "Estimation of Roll Motion Parameters using R-MISO System Identification Technique", eds., J.S. Chung, M. Muskulus, T. Kokkinis and A.M. Wang, *26th International Offshore and Polar Engineering (ISOPE 2016) Conference*, Vol. 3, 568-574, International Society of Offshore and Polar Engineers (ISOPE), Rhodes (Rodos), Greece.

Somayajula, A. and Falzarano, J.M. (2015b), "Validation of Volterra Series Approach for Modelling Parametric Rolling of Ships", *Proceedings of ASME 2015 34th International Conferences on Ocean, Offshore and Arctic Engineering*, American Society of Mechanical Engineers, St. John's, NL, Canada.

Somayajula, A., Guha, A., Falzarano, J., Chun, H.H. and Jung, K.H. (2014), "Added resistance and parametric roll prediction as a design criteria for energy efficient ships", *Int. J. Ocean Syst. Eng.*, **4**(2), 117-136.

Somayajula, A.S. and Falzarano, J.M. (2016c), "A comparative assessment of simplified models for simulating parametric roll", *J. Offshore Mech. Arctic Eng.*.

MK